Insights into the stability and thermal degradation of P3HT:C$_{60}$ blended films for solar cell applications

David E. Motaung · Gerald F. Malgas · Christopher J. Arendse

Abstract This paper demonstrates the changes in the nanoscale morphology of the blended films induced by a diffusion of C$_{60}$ molecules and degradation during longer thermal treatment above the glass transition temperature (130 °C). The results showed that the film morphology, including the size and population of poly(3-hexylthiophene) (P3HT) crystallites, rapidly reduced with annealing time. A large-scale (>1μm) C$_{60}$ aggregation, demonstrating a bulky phase separation between the polymer and C$_{60}$, was identified after 5 h annealing, which resulted in a degradation of charge carrier mobility and conductivity. X-ray diffraction verifies that the interchain packing of P3HT within the crystallized phase improved with an increasing in annealing time, but the volume fraction of the P3HT (100) phase normal to substrate increased up to 3 h and decreased at longer annealing times resulting in the ageing of the films. Changes in the infrared spectra of the extended annealed samples were recorded and the oxidation products were identified. A degradation mechanism that accounted for the modifications in the infrared spectra and a detachment of the hexyl chain from P3HT was demonstrated, resulting in chain cutting, conjugation loss and a reduction in the UV–vis absorbance. The morphology change with the annealing time resulted in an abrupt decrease in the PCE of P3HT:C$_{60}$ solar cells. These findings signify that the stability of P3HT:C$_{60}$ solar cells cannot be secured for longer annealing period owing to the unsettled morphology.

Introduction

Polymer solar cells based on conjugated polymers have been intensively investigated as a potential source of renewable electrical energy, since photo-induced electron transfer from conjugated polymer to fullerene was first reported in 1992 by Sariciftci et al. [1]. An exceptional improvement in the device performance of polymer solar cells has been made, as the architecture of the polymer solar cell has been changed from the Schottky barrier single layer [2] to the donor/acceptor bilayer and bulk heterojunction (BHJ) [3–5]. From a material point of view, blends of poly(3-hexylthiophene) (P3HT) and [6]-phenyl-C$_{61}$-butyric acid methyl ester (PCBM) are most widely used as an active layer. Various studies showed that the device performance based on these materials is strongly related to the nano-morphology of the blends, where van der Waals crystal packing of the molecules and the formation of nanoscale domains of the two phases are strongly dependent on the processing conditions, solvents used and finally on post-production treatment [5–8].

Power conversion efficiencies (PCEs) ranging between 5 and 6.5% have been reported for simple BHJ cells [4, 5] and for tandem cells [9], respectively, while the predictions of the theoretically and practically accessible PCEs are indicated to be around 10% [10, 11]. As an area of focus, the PCE is of course very important to compete with the more mature silicon technology and justify research in an inferior technology. However, significant improvement of stability and increase of lifetimes up to scales that could

D. E. Motaung · G. F. Malgas (✉)
DST/CSIR Nanotechnology Innovation Centre, National Centre for Nano-Structured Materials, Council for Scientific Industrial Research, P. O. Box 395, Pretoria 0001, South Africa
e-mail: gmalgas@csir.co.za

D. E. Motaung · C. J. Arendse
Department of Physics, University of the Western Cape, Private Bag X17, Bellville 7535, South Africa

comply with industrial standards are essential requirements for further progress and commercialization of organic solar cell devices [12–18].

To date, some of these criteria have been achieved individually, but they have not all been combined for the same material or material technology. Krebs et al. [14] reported stable solar cells with a lifetime in excess of 10,000 h under full sun (AM1.5), high temperature and with exclusion of oxygen and moisture. They also predicted an operational lifetime in excess of 20,000 h by using a thermal acceleration factor of 4 between 25 and 72 °C and indoor illumination intensities of 50–100 Wm^{-2} [13, 14]. Katz et al. [15] reported a most stable PV cell of P3CT-C$_{60}$ in outdoor testing. Krebs [17] reported a reasonable storability of a PV cell in ambient air without any form of encapsulation and continuous operation in air at 1000 Wm^{-2}, AM1.5, 72 ± 2 °C, 35 ± 5% relative humidity for 100 h to 80% of the initial performance. So far there have been few studies in the accelerated studies where the devices are subjected to extra stress in the form of high temperatures, high incident light intensities and continuous illumination [19–21]. However, the thermal stability on the morphology, structure and electrical properties, such as charge carrier mobility and conductivity, of P3HT blended with C$_{60}$ has not been fully addressed. In this paper, we investigate the thermal degradation of the P3HT:C$_{60}$ blended films during the long annealing times and correlate this with the chemical structure, morphology, charge carrier mobility and solar cell performance.

Experimental details

Sample preparation

Regioregular poly(3-hexylthiophene) (rr-P3HT) was used as a light absorption and electron donating material, while C$_{60}$ fullerene was used as an electron acceptor material. The molecular weight (M_n) of P3HT reported by Sigma-Aldrich was ~64,000 g mol^{-1}; with regularity that is greater than 98.5% for head-to-tail. These materials were used as received, without any further purification. Sample preparations were done according to the following procedure. Indium tin oxide (ITO)-coated glass (surface resistivity of 8–12 Ω sq^{-1}, transmittance >83%) and silicon (Si) (100) substrates were ultrasonically cleaned with organic solvents and detergents, and then rinsed in de-ionized water. Photoactive layers were prepared by mixing P3HT:C$_{60}$ in a 1:1 weight ratio and dissolving the constituents in either chloroform (CF) or dichlorobenzene (DCB). CF has a boiling point of 132.0 °C and a solubility of 0.16 mg mL^{-1} in C$_{60}$ fullerene, at room temperature [22]. To attain a complete dissolution between the polymer

and blends, the solutions were stirred overnight at 50 °C. It is worthy to mention that no sonication or filtering was used in this process, since it would adversely affect the polymer side chains and possibly lead to a decrease in the conjugation length of P3HT strands. The active layer consisting of the polymer and the blends was spin-coated on top of the ITO glass and Si substrates and dried at 50 °C for 15 min, to evaporate the excess solvent. To observe the thermal ageing (stability) of P3HT and the blended films, they were subjected to extra stress in the form of high-temperature annealing (130 °C) and times (0–30 h). For device fabrication a thin layer of poly(3,4-ethylenedioxy-thiophene):poly(styrenesulfonate) (PEDOT:PSS) solution was spin-coated onto the ITO glass substrates. This was followed by thermal treatment of the PEDOT:PSS/ITO substrates at 100 °C for 30 min. The active layer consisting of the polymer blends was spin-coated on top of the PEDOT:PSS/ITO glass substrates and dried at 50 °C for 15 min.

Characterization

To examine how the annealing sequence of the polymer photoactive layer is affecting the stability, atomic force microscopy (AFM) studies (Veeco AFM system, Digital Instruments) were carried out; to characterize the phase separation and the microstructure of the as-prepared and long-time annealed P3HT:C$_{60}$ films on the Si substrate. The microstructures of the blended films were studied using a Carl Zeiss Imager Z1M polarised optical microscope (POM). The films thickness (~90 nm) was measured using α-stepper Veeco DEKTAK$^{©}$ 6M Stylus profilimeter instrument. The degree of ordering of the P3HT domains were characterized by Panalytical X'pert PRO PW 3040/60 X-ray diffractometer equipped with a Cu K$_\alpha$ ($\lambda = 0.154$ nm) monochromated radiation source. The measurements were extracted at 45.0 kV and 40.0 mA. Data were obtained from $2\theta = 1°$ to 35° with a step size of 0.02°.

The Raman spectroscopy measurements were conducted at room temperature with a 514 nm excitation laser with a spectral resolution of 0.4 cm^{-1}. The structure of pure P3HT with different concentrations of C$_{60}$ prepared from CF and DCB solvents was characterized by Fourier transform infrared spectroscopy (FT-IR) using a Perkin Elmer FT-IR spectrometer. The conductivity and the mobility of the P3HT and blended films were extracted using a Hall Effect measurement system (ECOPI, HMS-3000). All measurements were performed at room temperature in air. The absorption spectra of the blended films were measured using a Varian Cary 1E ultra violet–visible (UV–vis) spectrometer.

Solar cells were completed by laminating a Platinum top electrode on top of an ITO glass substrate. This glass/Pt

substrate was placed on top of the ITO/PEDOT:PSS/ P3HT:C$_{60}$ substrate with an appropriate displacement and laminated together by applying a certain pressure at a controlled temperature using a hydrostatic pressurizer with hot plates (AH-1TC, ASONE, Japan). The current–voltage (I–V) characteristics were measured using a Keithley 4200 Semiconductor Characterization System. The devices were irradiated at 100 mW cm^{-2} using a xenon short arc lamp xenon lamp-based Sciencetech SF150 solar simulator with a power of 150 W. The optical power at the sample was 100 mW cm^{-2}, detected using a daystar meter. All the photovoltaic properties were evaluated in ambient air conditions at room temperature.
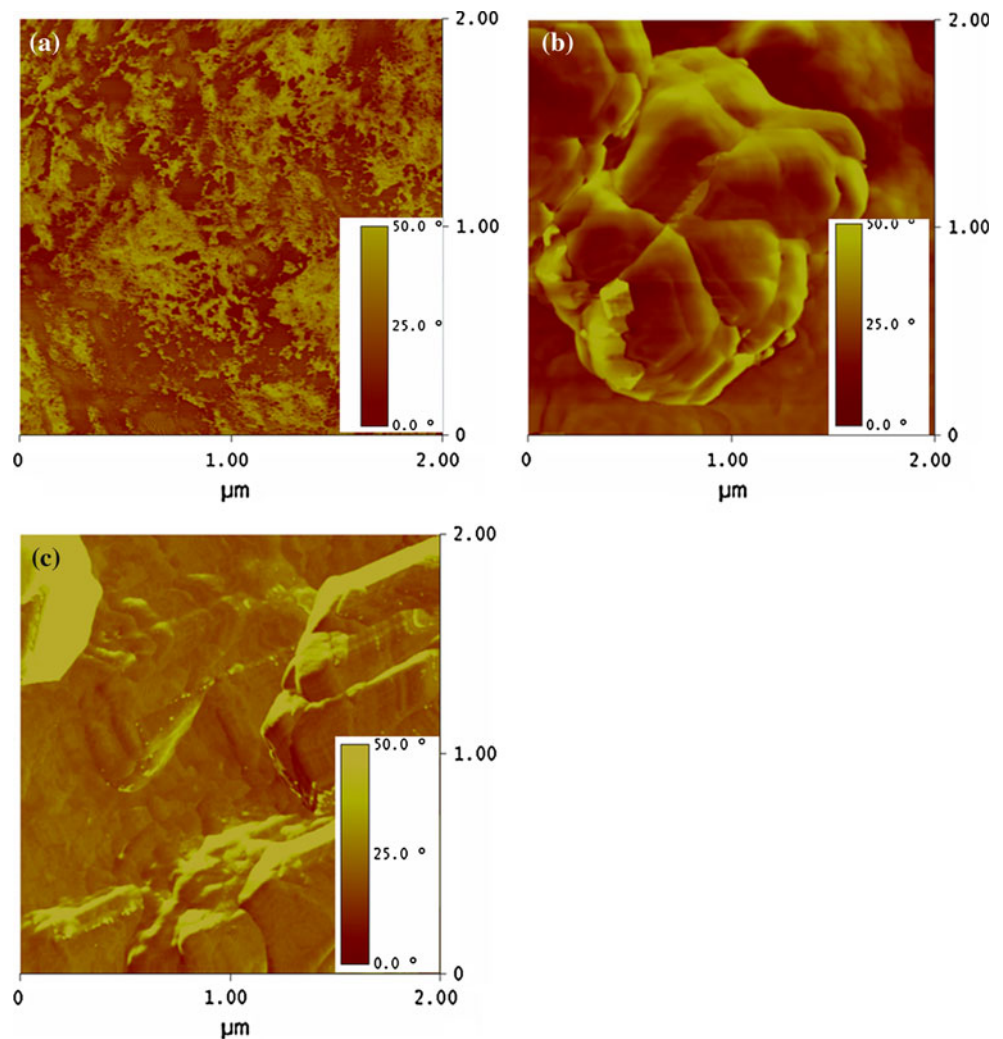
Results and discussion

Polymer-based organic solar cells are known to offer a poor stability in real use conditions, and the photo and thermal degradation of the active organic layer play an important role in the reduced lifetime of the devices. Figure 1 shows the phase images of the as-prepared P3HT: C$_{60}$ (1:1 wt. ratio) blended film spin-coated from chloroform solution and those annealed at long times. The as-prepared film is smooth with an atomically flat surface, Fig. 1a.

The surface roughness significantly increases with thermal annealing up to 30 h, Figs. 1b, c and 2, which are induced by overgrown large-scale C$_{60}$ clusters (or domains). The size of these domains varies from 200 nm up to tens of micrometres [23–25]. The roughening of the surface could be due to macro-scaled phase separation resulting from polymer self-organization into a disordered structure with fewer P3HT crystallites. Although the crystallites grew upon annealing, they flowed with the amorphous P3HT domains and increase the propagation of the P3HT:C$_{60}$ phase separation. The large phase separation may deteriorate the device performance.

Phase contrast optical microscopy on both blends prepared from either CF or DCB demonstrated that tiny clusters related to fullerene molecules diffuse out of the

Fig. 1 AFM phase images (2 m × 2 μm) of P3HT:C$_{60}$ (1:1 wt. ratio) films dissolved in CF, **a** as-prepared, **b** annealed for 5 h and **c** annealed for 30 h
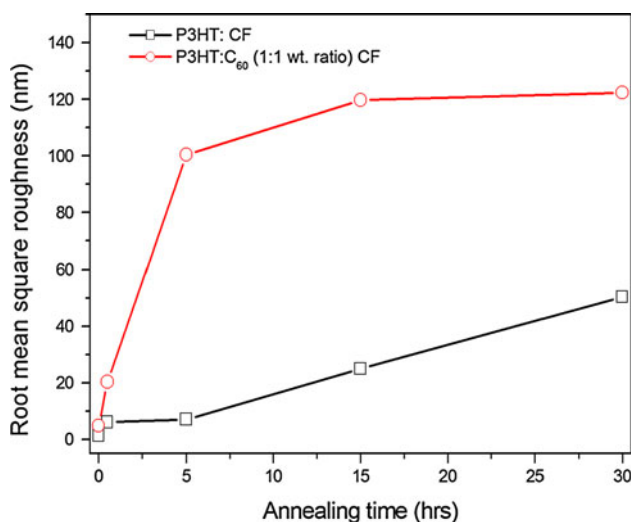
Fig. 2 Root mean square roughness values of the films as a function of annealing time

upper part of the blend film towards the nanoscopic C_{60} domains that are already present both in the lower regions of the spin-coated film and near the air surface after 10 h of annealing (Fig. 3b, e). After 30 h of exposure, tiny clusters surrounded the larger aggregates, and a further depletion or degradation in the C_{60} content within the upper, subsurface part of the blend layer was observed (Fig. 3f). Swinnen et al. [26] demonstrated that large PCBM clusters in blend films can rapidly grow up to a few hundred micrometres in length under a condition that accelerates PCBM diffusion, such as high-temperature annealing.

These results suggests that, although nanometer-scale phase separation of the donor/acceptor blend can be attained in the laboratory through device optimization, prolonged exposure to elevated temperatures will induce macrophase separation with micrometer scale and large surface roughness (Fig. 2). This could be due to the fact that the nanometer-scale phase separation in the blends of the conjugated polymer and the fullerene derivatives is not thermodynamically stable [27]. It is suggested that the macrophase separation may limit charge separation, which occurs at the donor–acceptor interface and thus lower the PCE in the photovoltaic device. The macrophase-separated domain size (>1 µm scale) observed for longer annealing time is much larger than the exciton diffusion length in conjugated polymers. It should be noted that the stability of P3HT and blended films at 130 °C (in this study) can be related to the long-term stability at low temperature (e.g. 25 °C, operating conditions of a solar cell) by an acceleration model based on the Arrhenius equation [19]: an increase in temperature accelerates molecular and segmental motions, bringing the system more rapidly to equilibrium (or apparent equilibrium), and therefore

short-time annealing at high temperature corresponds to long-time annealing at low temperature.

To investigate the effect of long-time annealing on the ageing and chain packing of P3HT in the blend films, the XRD patterns of P3HT and the P3HT:C_{60} blended films annealed at different times are shown in Fig. 4. Before annealing, the films show the (100) diffraction peak at $2\theta = 5.4°$, corresponding to an ordered lamellar structure with an interlayer spacing, which was formed by parallel stacks of P3HT main chains that were separated by the alkyl side chains, as shown in the inset of Fig. 4a [28]. The (100) peak intensity of the annealed films up to 5 h is much stronger than the as-prepared sample, while the diffraction peaks shifted to higher 2θ angles and a reduction in the full-width-at-half-maximum (FWHM) is observed. This results in a momentous decrease in the d-spacing, FWHM and an increase in the grain sizes of the (100) plane, as depicted in Fig. 5.

The decrease in the d-spacing with shorter annealing time suggests that inter-digitation or tilting of the side groups transpired during the formation of ordered aggregates in the solution and induced crystallization during film deposition. Motaung et al. [29] showed a decrease in the d-spacing with pre-annealed substrates prior to the active layer deposition. During longer annealing times (5–30 h), the peak intensity reduces and the diffraction peaks shift to lower angles presenting an increase in d-spacing and FWHM (Fig. 5b) and a decrease in grain size (Fig. 5c), which demonstrated a complete breakage of lamellar stacking of polythiophene induced by thermal stress. It is suggested that the volume fraction of the π-conjugated planes of P3HT (100) with lamella are oriented normal to the substrate [6, 30].

Therefore, the interchain packing of P3HT within the crystallized phase improved with an increasing in annealing time, but the volume fraction of the P3HT (100) phase normal to substrate increased up to 3 h and decreased at longer annealing time resulting in the degradation of the films. It is concluded that the P3HT crystallites turns out to be unstable due to enhanced thermal motion of the P3HT molecules at longer annealing times, which results in the "melting" of the P3HT crystallites and thus a reduction of the P3HT crystallinity as confirmed by the XRD and Raman analysis (Fig. 6). A reduction in the C=C stretching vibrations of the thiophene ring, C–C skeletal stretching and C–S–C ring deformation at 1440, 1380 and 720 cm^{-1} wavenumber [31–33] is observed with longer annealing times. This indicates the formation of disordered/less crystalline material with a slight reduction in the conjugation length as the annealing time increases. Simultaneously, the broadening of the FWHM of these peaks from 29.36 cm^{-1} (as-prepared) to 50.41 cm^{-1} (30 h annealed) also supports the reduction in the chain length.
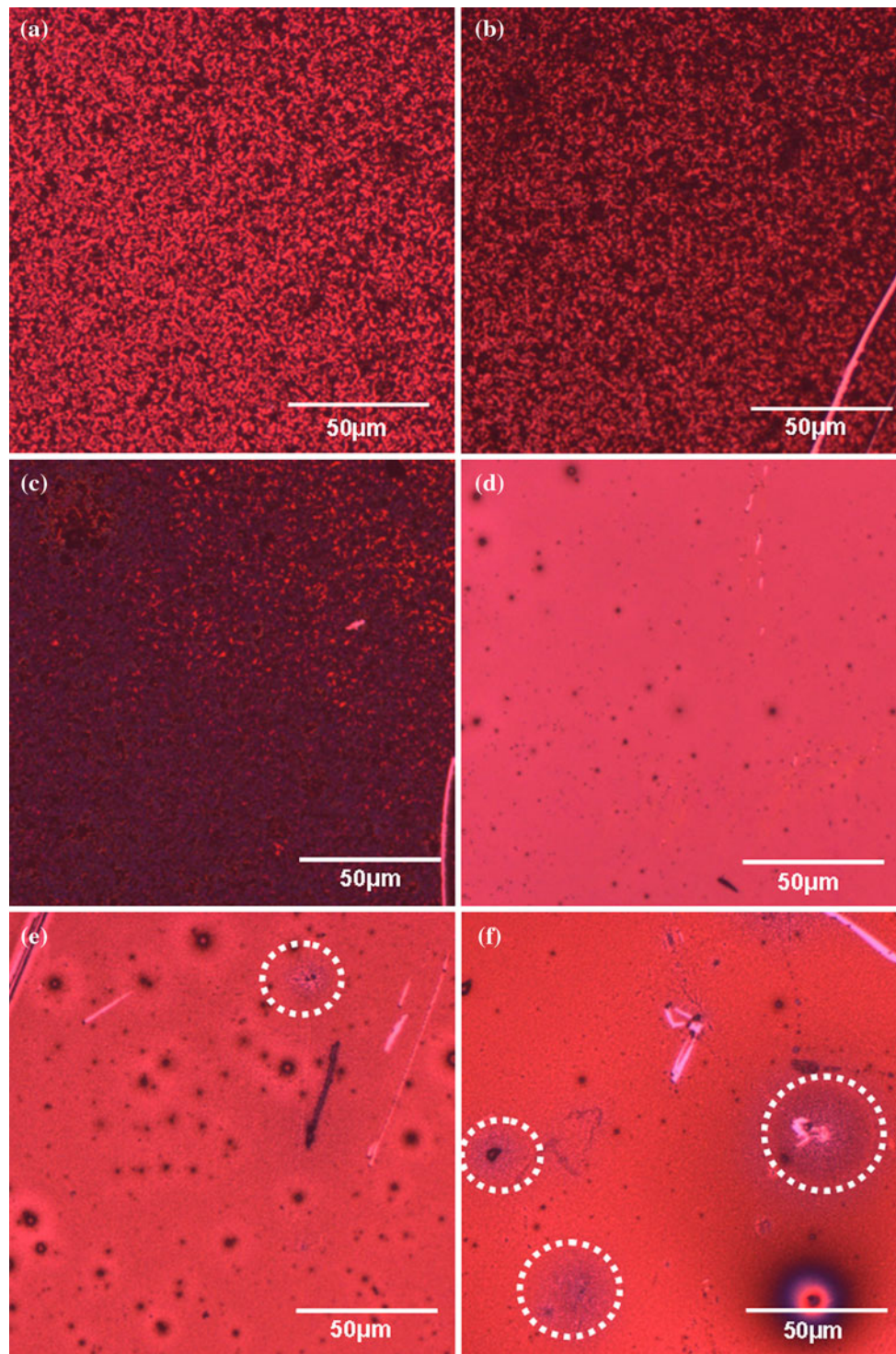
Fig. 3 Polarized optical micrographs of the surface of a P3HT:C$_{60}$ (1:1 wt. ratio) films prepared from CF, **a** as-prepared, 0 h; **b** 10 h; **c** 30 h while the images in **d**–**f** corresponds to as-prepared, 10 h, 30 h films prepared using DCB

Figure 7 shows the FT-IR spectra of the thermal degradation of P3HT and the blended film prepared from a chloroform solution. The peak at 2690 cm^{-1}, assigned to methyl asymmetric stretching vibration of the hexyl side chain, gradually reduces in intensity with an increase in

annealing time, which involves the detachment of the side chain from the P3HT backbone (Fig. 7a). Two other peaks at 2923 and 2855 cm^{-1}, corresponding to methylene in phase and out phase vibrations [34], also decrease in intensity with an increase in annealing time. After 5 h of
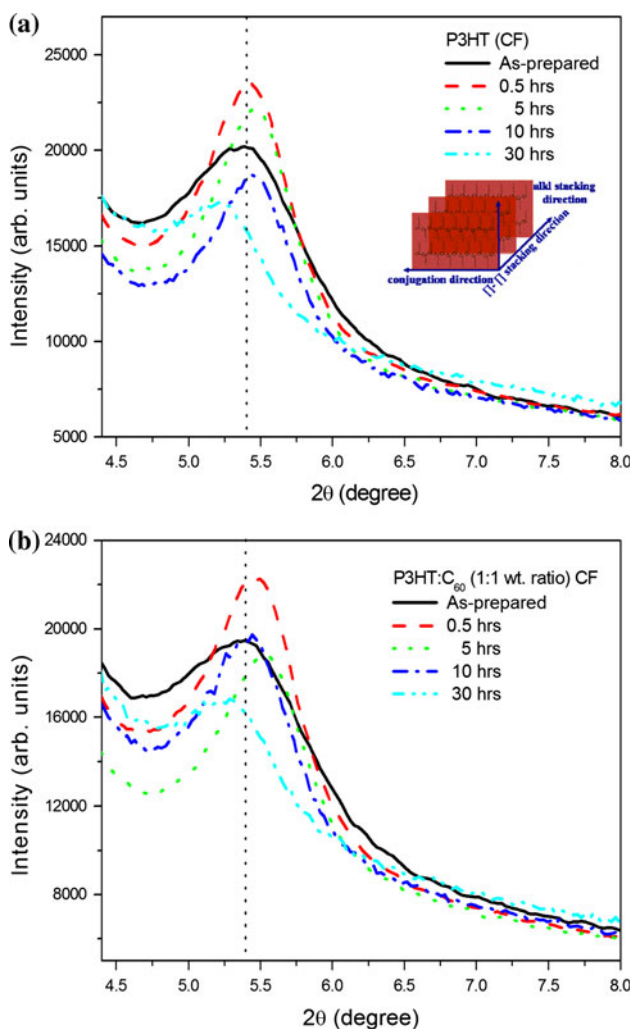
Fig. 4 Diffraction patterns of **a** rr-P3HT (CF) and **b** P3HT:C_{60} (1:1 wt. ratio) (CF). The *inset* depicts the orientation of the P3HT crystalline domains with respect to the substrate (**a**)
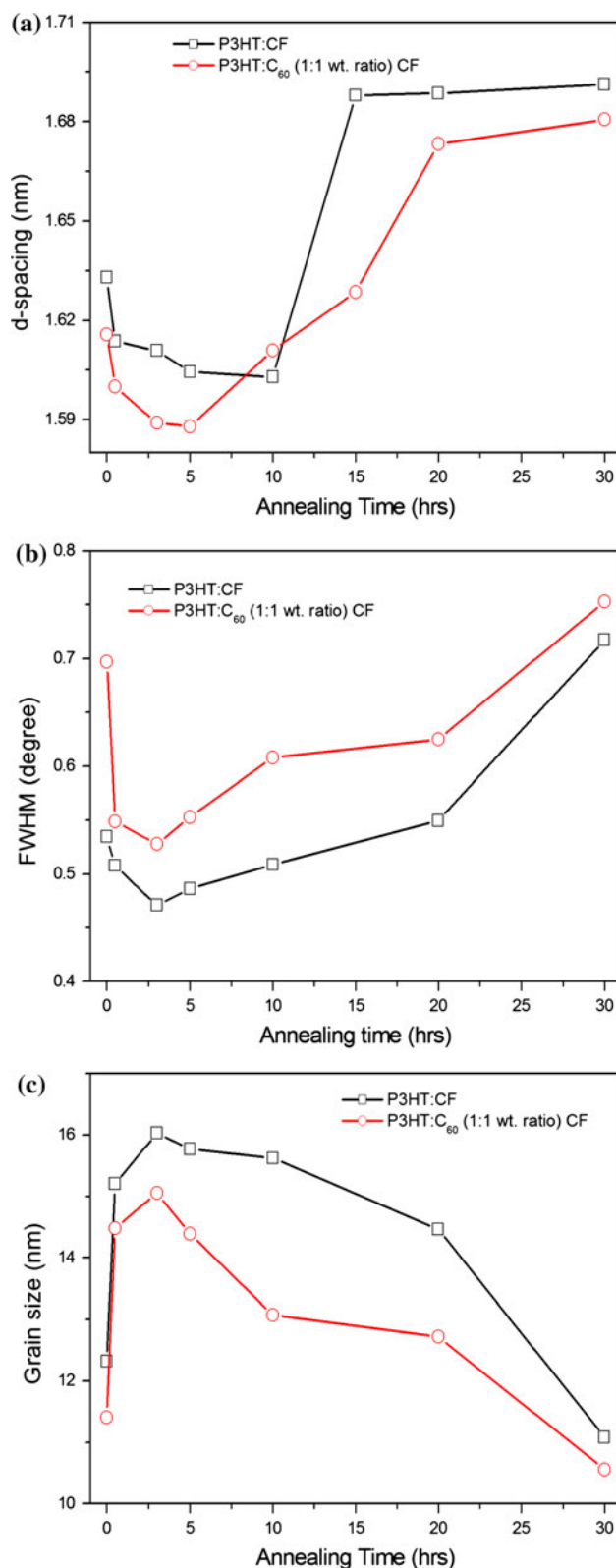

Fig. 5 Structural ageing of P3HT crystals during extended annealing **a** *d*-spacing, **b** FWHM of the P3HT (100) peak and **c** the average P3HT (100) crystal size
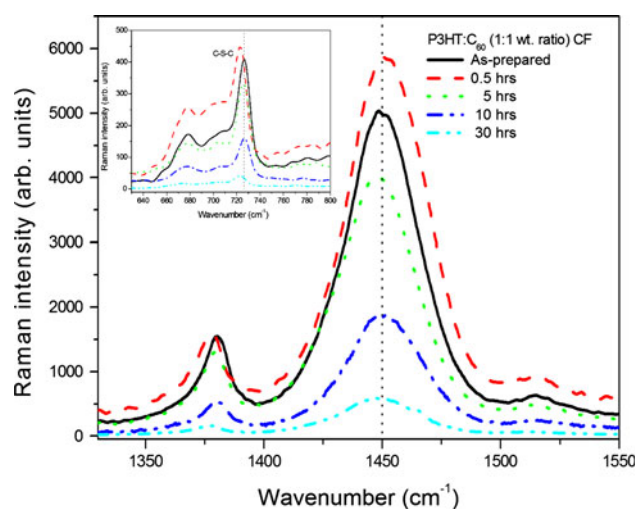
annealing a new shoulder arise around 2956 cm^{-1} and disappears with extended annealing time. At the same time, a new band (or shoulder) at 2870 cm^{-1} progressively developed with longer annealing exposure. Furthermore, a small shift in frequency and a total disappearance of the symmetric ring stretching mode peaks at 1457 cm^{-1} and the anti-symmetric C=C stretching peak 1510 cm^{-1} (circle) are observed with longer annealing times. Since the ratio between the intensity of the anti-symmetric C=C stretching peak and the intensity of the symmetric stretching peak can be used to probe the average conjugation length of P3HT [35–37], the results indicate that the conjugation length of P3HT chains is disrupted during longer annealing times (Fig. 7b, c). The signals at 1115 and 620 cm^{-1}, which corresponds to the S=O and S–O stretching frequencies of a sulphonic acid or ester

Fig. 6 Raman spectra of as-prepared and annealed films of P3HT:C_{60} (1:1 wt. ratio) spin-coated from CF

according to the literature data, arise during the 5–10 h annealing time (result not shown).

The peak at 668 cm^{-1}, assigned to the C–S stretching in pre-treated P3HT and blended films, disappears during longer annealing time, indicating the loss of the C–S units. A similar degradation on the P3HT structure (alkyl groups and thiophene rings) was observed by Manceau et al. [38, 39] when exposing the polymer under UV–visible light and thermal ageing. Moreover, one can observe the formation of thermal products in the carbonyl region (Fig. 7c). A band is detected at 1782 cm^{-1} and a broadening appears near the region 1700–1710 cm^{-1}, which is attributed to C_{60} moiety [40]. This conclusion is confirmed by the fact that the degradation of C_{60} also provokes the development of a band at 1782 cm^{-1} accompanied by another one at 1745 cm^{-1}. It can be concluded that a gradual decrease in intensities of the FT-IR peaks in the finger print region indicates a thermal degradation of P3HT with increasing in annealing exposure [41].

Figure 8 demonstrates the Hall mobility and conductivity of P3HT and blended films prepared from chloroform and dichlorobenzene solutions during long annealing times. An increase in the mobility and conductivity of the P3HT and the blended films is observed after short anneals. Such an increase, especially in the case of the blends, may be attributed to enhanced polymer ordering, since C_{60} crystallizes out of the polymer matrix under optimized annealing conditions [42–44], leaving the polymer chains behind that will endeavour to reorganize and obtain an optimized morphology. It is clear that films spin-coated from CF disclose a higher mobility and conductivity compared to films spin-coated from DCB. It is assumed that the improved electrical properties spin-coated from CF are induced by smaller polymer and fullerene clusters
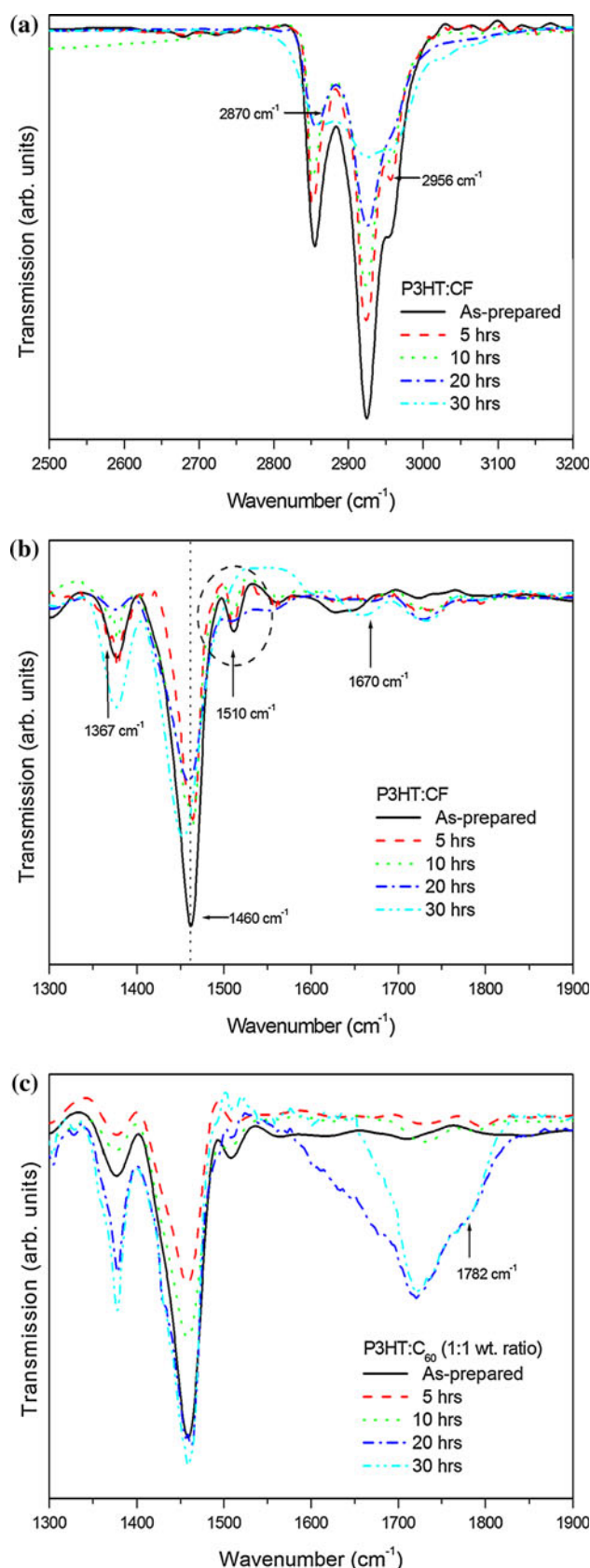

Fig. 7 FT-IR spectra of as-prepared P3HT and P3HT:C_{60} (1:1 wt. ratio) films compared with that annealed at 130 °C for different times

formed during spin-coating, which lead to the development of continuous pathways for charge carriers and an increase in the interfacial area that enhances the exciton dissociation [45]. It is interesting to note that, during longer annealing times (5–25 h), a considerable decrease in both the mobility and conductivity were observed. It is suggested that the changes in the mobility and conductivity could be due to a depletion of P3HT and C_{60}. Furthermore, it can be concluded that the decrease in mobility is attributed to the formation of large clusters during longer annealing times as observed in the POM, XRD and AFM analysis.

The UV–vis absorbance spectra (Fig. 9) show a blue-shift and a complete reduction in the absorbance with an increase in annealing time, indicating that the thermal degradation aggravates the modification of the chemical structure of chromophore groups and reduces the conjugation length of P3HT. This is in good agreement with the FT-IR results obtained and discussed in Fig. 7. Thermal

degradation also altered the degree of inter-chain order in the microcrystalline domains of P3HT, as shown by the disappearance of the shoulder at 600 nm for the P3HT films dissolved using dichlorobenzene. This could be due to the higher solubility of P3HT and C_{60} in DCB, thereby inducing a finer phase separation and smaller grain size [46].

Through analysis of the P3HT:C_{60} film degradation process, the obtained data allowed us to propose a degradation mechanism that accounted for the formation of the different oxidative species due to the impact of thermal annealing on the polymer blends. Figure 10 shows a two step pathway for the degradation of the blends. In step 1 (Scheme 1), thermal degradation of P3HT as observed in Raman and FT-IR analyses starts approximately after an annealing time of 5 h. The results establish that P3HT starts to degrade with the detachments of lighter fragments like C–S units, as confirmed by the Raman and UV–vis
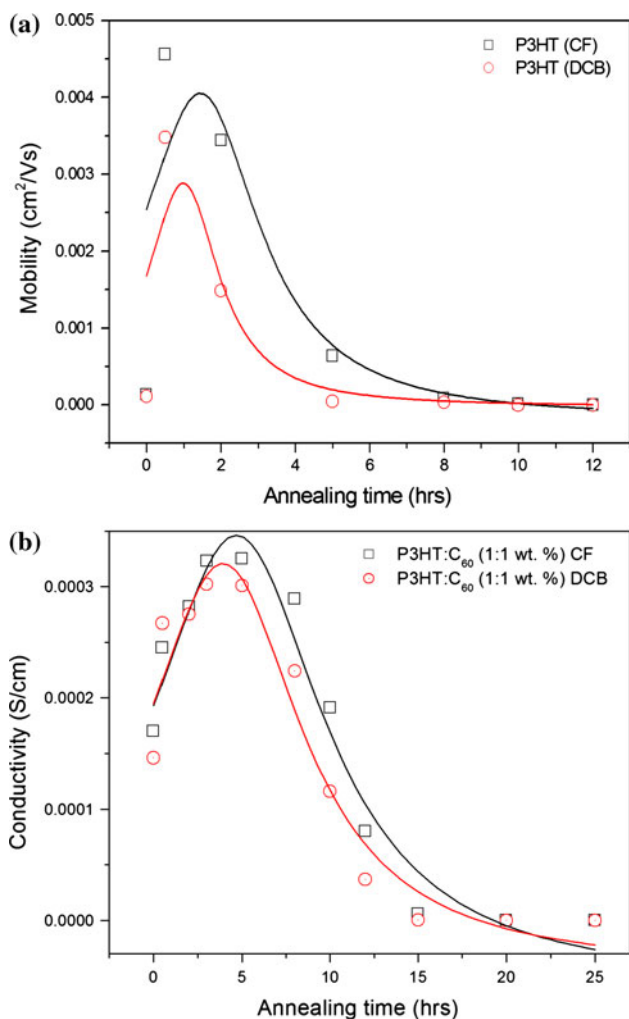

Fig. 8 Hall Effect a mobility of as-prepared and annealed films of P3HT and b electrical conductivity extracted from blended films. Solid lines are a visual guide of the behaviour
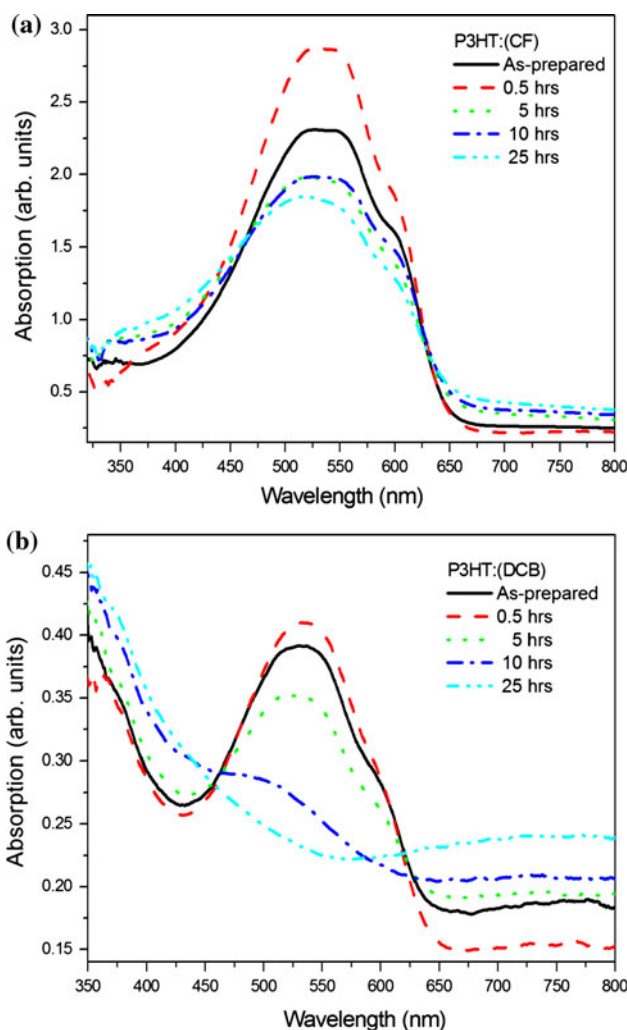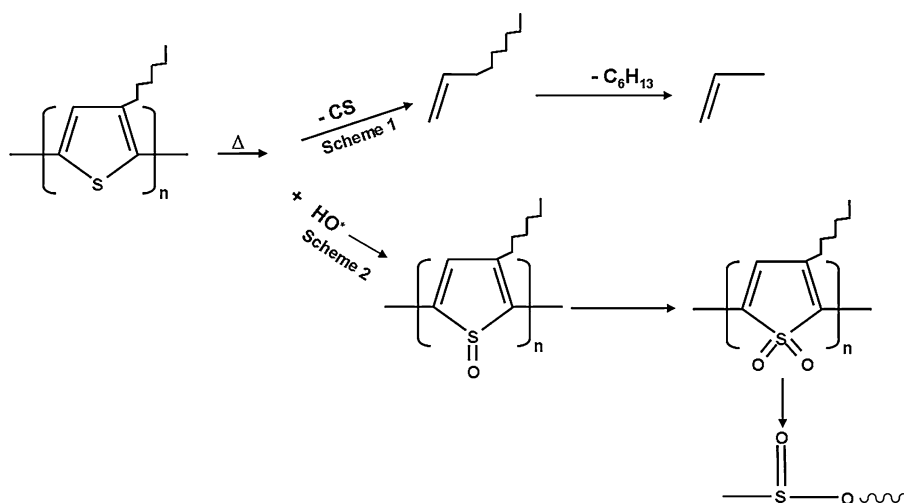

Fig. 9 UV–visible absorption spectra of the as-prepared and annealed films of a P3HT (CF) and b P3HT (DCB) films

Fig. 10 The probable pathway
followed by the thermal
degradation of a P3HT polymer

analyses, with the modification of the chemical structure of
chromophore groups, which results in a reduction of the
conjugation length of P3HT. A thermal decomposition of
the C–S units of polythiophene on pyrolysis mass pho-
tometry at a very low temperature (~ 50 °C) has also been
reported by Vatansever et al. [47]. The degradation after
30 h is due to the subsequent loss of C_6H_{13} detached from
the polymer backbone. POM results showed that after 30 h
of exposure, tiny clusters that surrounded the larger poly-
mer and C_{60} aggregates, depletes or degrades. Reddy et al.
[48] demonstrated that the final products of C_2H_2 units
after CS and C_6H_{13} detached from the polymer backbone
resulted in amorphous carbon and a mixture of fullerenes.

Degradation products of FT-IR stretching frequencies
(1115 and 620 cm^{-1}) have also been identified after 10 h
of annealing as shown in Fig. 10 (Scheme 2). Rivaton et al.
[49] indicated sulphinate moieties can be formed by
sulphone degradation, as observed in the case of polysul-
phone. It is also known that sulphur atoms can be readily
oxidized by hydroxyl radicals ($OH^\bullet$) to form sulphoxides
and sulphones [50]. The characteristic IR vibrations of
sulphoxides (1045 cm^{-1}) have been detected. Therefore, it
is possible that the sulphur atom of the thiophene ring is
initially oxidized into sulphoxides, then into sulphones that
are later decomposed into sulphinate esters.

To understand the degradation mechanism on the pho-
tovoltaic device performance, the current density voltage
(I–V) curves of the devices annealed for different times are
shown in Fig. 11. It is evident from Fig. 11 and Table 1
that the as-prepared device exhibits a low PV performance
with a short circuit current density (I_{sc}) of 29.67 µA cm^{-2},
fill factor (FF) of 0.15, open circuit voltage (V_{oc}) of 0.32 V
and PCE of 0.014%. After annealing for 30 min, the I_{sc} and
FF increased remarkably resulting to a PCE 0.048%. This
increase in the PCE is due to the improved absorption of
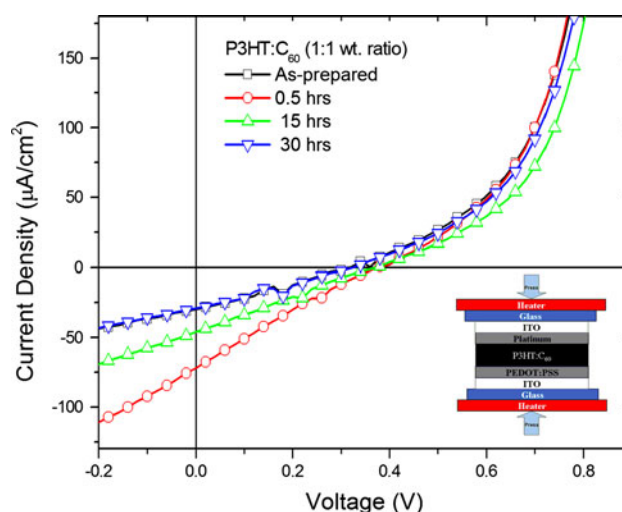the incident light (Fig. 9) and the charge transportation

Fig. 11 I–V curves for devices processed from P3HT:C_{60} and
annealed at 130 °C for different times

Table 1 Photovoltaic devices performance of blended structures

Annealing time (h)	I_{sc} (µA cm^{-2})	V_{oc} (V)	FF	PCE (%)
As-prepared	29.67	0.32	0.15	0.014
0.5	72.84	0.35	0.19	0.048
15	47.84	0.35	0.16	0.027
30	28.73	0.36	0.14	0.015

property (Fig. 8) of the highly ordered P3HT:C_{60} structure.
The C_{60}-rich region reduces the recombination losses and
increases the current density [51–53]; thus increasing the
performance of the solar cell after annealing.

Upon annealing for longer times the performance of the
solar cell reduced considerably (Table 1). This is due to a
degradation ordering of P3HT, the deficient C_{60} molecules
that accepted the generated electrons, and the deteriorated
phase separation resulting from the formation of the large

C_{60} aggregates/clusters (Fig. 1) through the high-temperature annealing. The larger C_{60} cluster does not only induce a large-scale phase separation between P3HT and C_{60}, but also a rough P3HT:C_{60} (1:1 wt ratio) blend film as depicted in Fig. 1. The rough P3HT:C_{60} layer may form some shunt paths after the top electrode deposition, resulting in a low open circuit voltage [54].

Conclusion

Alterations in the nano-scale morphology of the blend films of P3HT and blended films induced by a diffusion of C_{60} molecules and degradation during longer thermal treatment above glass transition temperature was observed. Distinct degradation kinetics and morphological changes that indicate the occurrence of different underlying physico-chemical mechanisms were observed. A large-scale (>1μm) C_{60} aggregation denoting large phase separation between the donor and acceptor, was identified, which arose after 5 h annealing. Alterations on the micro-structure resulted in the degradation of grain sizes, charge carrier mobility and electrical conductivity. FT-IR indicated that under extended thermal annealing the alkyl groups and thiophene rings vanish. The results establish that P3HT starts to degrade at early annealing stages (5 h) with detachments of lighter fragments like C–S units, followed by the abstraction of hydrogen attached to a carbon atom that is adjacent to a double bond, leading to backbone, side chain and sulphur oxidations. Chain scissions, conjugation loss and a decrease in the UV–visible absorbance arise from these reactions. The morphology change with the annealing time resulted in an abrupt decrease in the PCE of P3HT:C_{60} solar cells. The stability of P3HT:C_{60} solar cells cannot be secured for longer annealing period owing to the unsettled morphology and structure.

References

1. Sariciftci NS, Smilowitz LB, Heeger AJ, Wudl F (1992) Science 258:1474
2. Antoniadis H, Hsieh BR, Abkowitz MA, Jenekhe SA, Stolka M (1994) Synth Met 62:265
3. Tang CW (1986) Appl Phys Lett 48:183
4. Ryu MS, Cha HJ, Jang J (2010) Curr Appl Phys 10:S206
5. Ma W, Yang C, Gong X, Lee KH, Heeger AJ (2005) Adv Funct Mater 15:1617
6. Kim Y, Cook S, Tuladhar SM, Choulis SA, Nelson J, Durrant JR, Bradley DDC, Giles M, Mcculloch I, Ha C-S, Ree M (2006) Nat Mater 5:197
7. Hoppe H, Sariciftci NS (2006) J Mater Chem 16:45
8. Kim Y, Choulis SA, Nelson J, Bradley DDC, Cook S, Durrant JR (2005) J Mater Sci 40:1371. doi:10.1007/s10853-005-0568-0
9. Kim JY, Lee K, Coates NE, Moses D, Nguyen T-Q, Dante M, Heeger AJ (2007) Science 317:222
10. Koster LJA, Mihailetchi VD, Blom PWM (2006) Appl Phys Lett 88:093511
11. Scharber MC, Muhlbacher D, Koppe M, Denk P, Waldauf C, Heeger AJ, Brabec CJ (2006) Adv Mater 18:789
12. Lungenschmied C, Dennler G, Neugebauer H, Sariciftci NS, Glatthaar M, Meyer T, Meyer A (2007) Sol Energy Mater Sol Cells 91:379
13. Krebs FC, Spanggaard H (2005) Chem Mater 17:5235
14. Krebs FC, Norrman K (2007) Prog Photovolt Res Appl 15:697
15. Katz EA, Gevorgyan S, Orynbayev MS, Krebs FC (2007) Eur Phys J Appl Phys 36:307
16. Padinger F, Fromherz T, Denk P, Brabec CJ, Zettner J, Hierl T, Sariciftci NS (2001) Synth Met 121:1605
17. Krebs FC (2008) Sol Energy Mater Sol Cells 92:715
18. Jørgensen M, Norrman K, Krebs FC (2008) Sol Energy Mater Sol Cells 92:686
19. Schuller S, Schilinsky P, Hauch J, Brabec CJ (2004) Appl Phys A 79:37
20. De Bettignies R, Leroy F, Firon M, Sentein C (2006) Synth Met 156:510
21. Bertho S, Janssen G, Cleij TJ, Conings B, Moons W, Gadisa A, D'Haena J, Goovaerts E, Lutsen L, Manca J, Vanderzande D (2008) Sol Energy Mater Sol Cells 92:753
22. Ruoff RS, Tse DS, Malhotra R, Lorents DC (1993) J Phys Chem 97:3379
23. Chirvase D, Parisi J, Hummelen JC, Dyakonov V (2004) Nanotechnology 15:1317
24. Klimov E, Li W, Yang X, Hoffmann GG, Loos J (2006) Macromolecules 39:4493
25. Savenije TJ, Kroeze JE, Yang X, Loos J (2005) Adv Funct Mater 15:1260
26. Swinnen A, Haeldermans I, van de Ven M, D'Haen J, Vanhoyland G, Aresu S, D'Olieslaeger M, Manca J (2006) Adv Funct Mater 16:760
27. Miyanishi S, Tajima K, Hashimoto K (2009) Macromolecules 42:1610
28. Erb T, Zhokhavets U, Gobsch G, Raleva S, Stuhn B, Schilinsky P, Waldauf C, Brabec CJ (2005) Adv Funct Mater 15:1193
29. Motaung DE, Malgas GF, Arendse CJ, Malwela T (2010) Mater Chem Phys 124:208
30. Li G, Yao Y, Yang H, Shirotriya V, Yang G, Yang Y (2007) Adv Funct Mater 17:1636
31. Motaung DE, Malgas GF, Arendse CJ, Mavundla SE, Oliphant CJ, Knoesen D (2009) Sol Energy Mater Sol Cells 93:1674
32. Brown PJ, Thomas DS, Kohler A, Wilson JS, Kim J-S, Ramsdale CM, Sirringhaus H, Friend RH (2003) Phys Rev B 67:064203
33. Malgas GF, Arendse CJ, Mavundla SE, Cummings FR (2008) J Mater Sci 43:5599. doi:10.1007/s10853-008-2797-5
34. Han Z, Zhang J, Yang X, Zhu H, Cao W (2010) J Mater Sci 45:3866. doi:10.1007/s10853-010-4442-3
35. Furukawa Y, Akimoto M, Harada I (1987) Synth Met 18:151
36. Trznadel M, Pron A, Zagorska M, Chrzaszcz R, Pielichowski J (1998) Macromolecules 31:5051
37. Motaung DE, Malgas GF, Arendse CJ, Mavundla SE, Knoesen D (2009) Mater Chem Phys 116:279
38. Manceau M, Rivaton A, Gardette J-L, Guillerez S, Lemaıtre N (2009) Polym Degrad Stab 94:898
39. Manceau M, Chambon S, Gardette J-L, Guillerez S, Lemaitre N (2010) Sol Energy Mater Sol Cells 94:1572
40. Chambon S, Rivaton A, Gardette J-L, Firon M (2007) Sol Energy Mater Sol Cells 91:394

41. Gustafsson G, Inganas O, Nilsson JO (1989) Synth Met 28:427
42. Motaung DE, Malgas GF, Arendse CJ, Mavundla SE, Oliphant CJ, Knoesen D (2009) J Mater Sci 44:3192. doi:10.1007/s10853-009-3425-8
43. Gong SC, Jang SK, Ryu SO, Jeon H, Park H-H, Chang HJ (2010) Curr Appl Phys 10:e192
44. Kumar A, Li G, Hong Z, Yang Y (2009) Nanotechnology 20:165202
45. Kwong CY, Djurisic AB, Chui PC, Cheng KW, Chan WK (2004) Chem Phys Lett 384:372
46. Motaung DE, Malgas GF, Arendse CJ (2010) Synth Met 160:876
47. Vatansever F, Akbulut U, Toppare L, Hacaloglu J (1996) Polymer 37:1103
48. Reddy PK, Goutam PJ, Singh DK, Ghoshal AK, Iyer PK (2009) Polym Degrad Stab 94:1839
49. Rivaton A, Gardette JL (1999) Polym Degrad Stab 66:385
50. Barnes I, Hjorth J, Mihalopoulos N (2006) Chem Rev 106:940
51. Qiao F, Liu A, Hu Z, Liu Y, Yu S, Zhou Z (2009) J Mater Sci 44:3462. doi:10.1007/s10853-009-3461-4
52. Reyes-Reyes M, Kim K, Carroll DJ (2005) Appl Phys Lett 87:083506
53. Shilkler R, Chiesa M, Friend RH (2006) Marcomolecules 39:5393
54. Motaung DE, Malgas GF, Arendse CJ (2010) J Mater Sci 45:3276. doi:10.1007/s10853-010-4339-1